Energy based simulation of a Timoshenko beam in non-forced rotation. Influence of the piano hammer shank flexibility on the sound.

Juliette Chabassier[a,b], Marc Duruflé[a,c]

[a] *Magique 3D Team, Inria Bordeaux Sud Ouest, 200 avenue de la vieille tour, 33 405 Talence Cedex, France.*
[b] *Laboratoire de Mathématiques Appliquées, CNRS UMR 5142, Avenue de l'Université, 64013 Pau, France.*
[c] *Institut de Mathématiques de Bordeaux, UMR 5251, Université Bordeaux 1, 351 cours de la Libération, 33 405 Talence Cedex, France.*

Abstract

A nonlinear model for a vibrating Timoshenko beam in non-forced unknown rotation is derived from the virtual work principle applied to a system of beam with mass at the end. The system represents a piano hammer shank coupled to a hammer head. An energy-based numerical scheme is then provided, obtained by non classical approaches. A major difficulty for time discretisation comes from the nonlinear behavior of the kinetic energy of the system. This new numerical scheme is then coupled to a global energy-preserving numerical solution for the whole piano. The obtained numerical simulations show that the pianistic touch clearly influences the spectrum of the piano sound of equally loud isolated notes. These differences do not come from a possible shock excitation on the structure, nor from a changing impact point, nor a "longitudinal rubbing motion" on the string, since neither of these features are modeled in our study.

Keywords: flexible piano hammer shank, piano model, pianistic touch, implicit time discretization, vibrating Timoshenko beam, energy preservation
2011 MSC: 35L05, 35A35, 35A40, 74K05

1. Motivation

Experimental studies [1, 2] tend to conclude that "the difference between two equally loud piano tones due to type of touch lies in the different noise components involved in the keystroke" (from [2]). This "noise" is supposed to come from the shock excitation of the piano structure (keybed, rim, iron plate). The authors seem to exclude any other mechanism explaining an influence of the pianistic touch on the resulted piano sound. However, experimental observations of [3, 4, 5] suggest that the vibration of the hammer shank plays a significant role in the interaction between the piano hammer and the string without being able to quantify its effect on the sound. Different possible mechanisms have been suggested, as a change in the striking position or a rubbing motion in the elongation direction of the string [3]. But the most frequent suggestion is that the shank vibrations contribute to the interacting hammer head - string force, and this is the mechanism that we wish to investigate in this article. Recently, numerical experiments have highlighted the influence of the hammer shank's flexibility on the whole piano action [6] and on the interaction between the hammer head and the strings [7]. To our knowledge, there is no published work which shows numerical experiments of a flexible hammer shank coupled with a whole piano (strings, soundboard and sound radiation in the air), therefore showing the influence of the shank flexibility on the resulting sound.

The aim of this work is to provide a complete physics based modeling and numerical solution of the interaction between a flexible hammer shank and a hammer head, using only constitutive laws. Our goal is also to design an energy-based numerical solution method, such that the numerical methods will ensure the preservation (or decay) of a discrete energy approximating the mechanical energy of the continuous system. Coupling this new numerical

Email addresses: juliette.chabassier@inria.fr (Juliette Chabassier), marc.durufle@inria.fr (Marc Duruflé)

method to the energy-preserving numerical solution for the other parts of the piano described in [8] (beginning with the strings, but also a soundboard and sound radiation in the free space) will thus be easily possible in a stable and physically relevant way. As a result, we will be able to provide several piano sounds obtained with the exact same configuration, where only the input forces (associated to different pianistic touches) will be changed. Moreover, our simulations do not model the shock on the structure. The impact point will be exactly the same is all simulations, and none of them implement a "longitudinal rubbing motion" of the hammer head on the string. Differentiating physical phenomena is a powerful feature of numerical experiments that cannot be done in a real experimental setup. Therefore the observed differences on these sounds will be attributed to the touch only.

A rotating Timoshenko beam will represent the flexible hammer shank. The beam will be in interaction with a mass located at its extremity representing the hammer head. The "macroscopic" motion of the beam is a rotation, the rotation angle being an unknown of the problem. The "microscopic" motions of the beam are small vibrations that can be viewed as small perturbations around the macroscopic position. The interacting forces acting between the hammer head and the hammer shank will be considered as Lagrange multipliers of the system. The obtained system of equations will involve nonlinear terms that will arise from the rotation of the coordinates system. We will see that some of them can be neglected, but the problem will remain challenging to solve numerically.

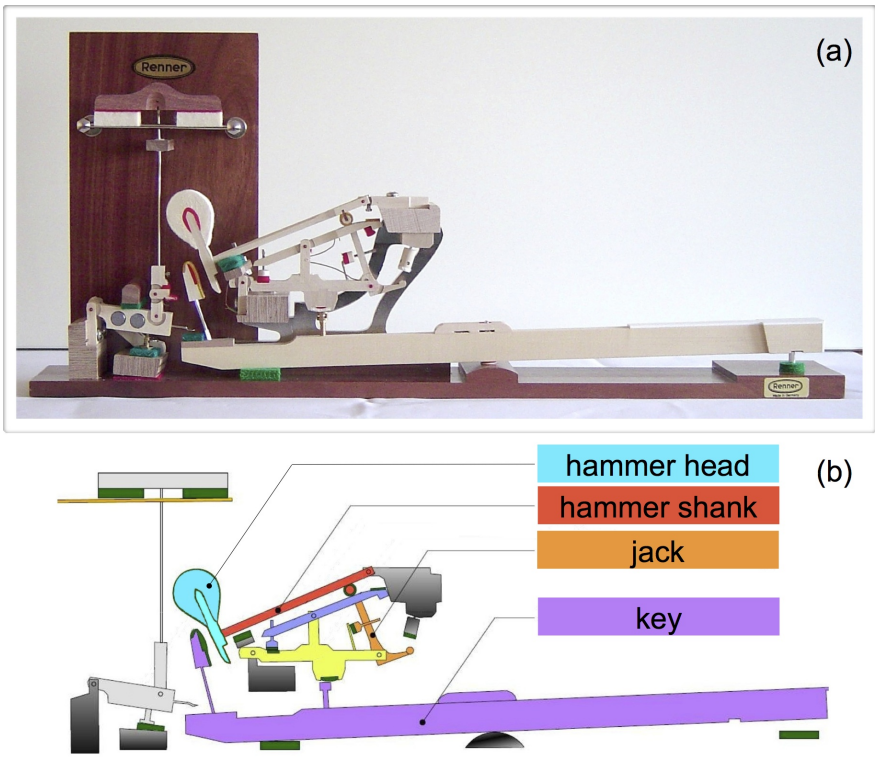

Figure 1: Grand piano action. (a) Photography of an isolated Renner grand piano action, from *kungfubrothers.com*. (b) Sketch of the different parts of the grand piano action, from *andersthorin.com*. When the player hits the key, the jack pushes the hammer shank near its fixation point and forces it into a rotating motion.

The mechanical system that we consider is a small part of the grand piano action (see figure 1) and consists of two parts:

- **the hammer shank**, in which we consider linear beam vibrations around a macroscopic position, written in

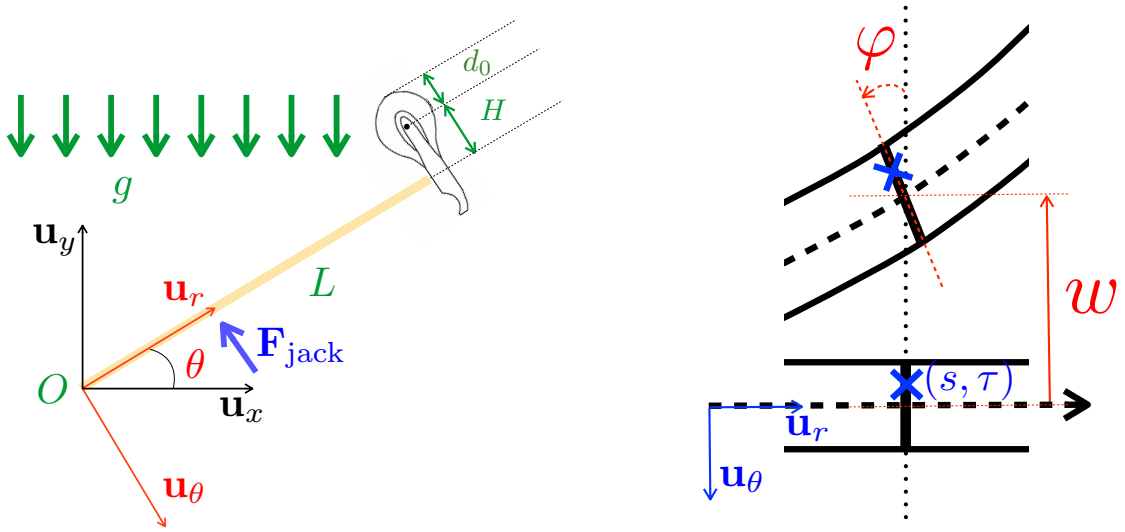

(a) Schematic view of the mechanical system.

(b) Schematic view of the shank configuration

Figure 2: Introduction of the notations.

rotating coordinates. It is subject to gravity, a "pushing" force (coming in reality from the contact with the jack), and a force at its extremity coming from the hammer head.

- **the hammer head**, not flexible, attached to the free end of the beam (cinematic continuity). It is subject to gravity, acts back on the hammer shank, and interacts with the strings.

Though the final goal of this work is to model the coupling of this mechanical system with piano strings, in the two first parts of this article we will simplify the problem and suppose that the forces coming from the coupling with strings are given data of the problem. In the third part of this article, we will provide numerical examples where the hammer shank and head have been coupled to the strings, the soundboard and the sound radiation, by treating the hammer head / string coupling in a mathematical weak way using Lagrange multipliers and computing the interaction forces from a crushing felt law as in [8].

2. A model for the { shank – head } mechanical system

We consider the notations of figure 2(a). The origin O is located at coordinates $(x_0, y_0, z_0) = (0, 0, 0)$ in the cartesian reference frame $(\mathbf{u}_x, \mathbf{u}_y, \mathbf{u}_z)$ This point will be fixed, since the only macroscopic motion of the shank that we consider is a rotation, with an angle θ.
In the following of this article, we will consider that all exterior forces are in the $(\mathbf{u}_x, \mathbf{u}_y)$ plane, therefore the displacement field will occur in this plane. Thus, we will only seek mechanical solutions in the $(\mathbf{u}_x, \mathbf{u}_y)$ plane. We denote the three unit vectors :

$$\mathbf{u}_r = \begin{bmatrix} \cos\theta \\ \sin\theta \\ 0 \end{bmatrix}, \qquad \mathbf{u}_z = \begin{bmatrix} 0 \\ 0 \\ 1 \end{bmatrix}, \qquad \mathbf{u}_\theta = \begin{bmatrix} \sin\theta \\ -\cos\theta \\ 0 \end{bmatrix}$$

The system $(\mathbf{u}_\theta, \mathbf{u}_r)$ is orthonormal, we denote by (s, τ) the coordinates of the undeformed configuration in this system (see figure 2(b)).

Following Timoshenko theory [9], which states that straight cross-sections remain straight during the deformation, the displacement of the beam's cross-section defined by $\{s\,\mathbf{u}_r + \tau\,\mathbf{u}_\theta,\ \tau \in (-R, R)\}$ is chosen of the form:

$$\mathbf{r} \;=\; (s - \tau \sin\varphi)\,\mathbf{u}_r \;+ (w + \tau\cos\varphi)\,\mathbf{u}_\theta \tag{1}$$

with w the deflection of the neutral fiber of the beam and φ the rotational angle of the cross section. The axis of rotation of the beam is equal to $\mathbf{\Omega} \;=\; \mathbf{u}_z$. The vectors $\mathbf{u}_r$ and $\mathbf{u}_\theta$ are not constant over time (in the sequel we shall denote $\dot{x}$ the time derivative of any quantity x):

$$\dot{\mathbf{u}}_r \;=\; \dot\theta\,\mathbf{\Omega}\times\mathbf{u}_r \;=\; -\dot\theta\,\mathbf{u}_\theta, \quad \dot{\mathbf{u}}_\theta \;=\; \dot\theta\,\mathbf{\Omega}\times\mathbf{u}_\theta \;=\; \dot\theta\,\mathbf{u}_r$$

And the second order time derivatives of these vectors read:

$$\ddot{\mathbf{u}}_r \;=\; -\dot\theta^2\,\mathbf{u}_r \;-\; \ddot\theta\,\mathbf{u}_\theta, \quad \ddot{\mathbf{u}}_\theta \;=\; -\ddot\theta\,\mathbf{u}_r \;-\; \dot\theta^2\,\mathbf{u}_\theta$$

The wooden part of the head is assumed to be rigid, hence the center of gravity of the mass (hammer head) at the end of the beam is parametrized by:

$$\boldsymbol{\xi} = L\,\mathbf{u}_r + \;(w(L) - H)\;\mathbf{u}_\theta \tag{2}$$

The top of the hammer head which can be in contact with the strings is parametrized by:

$$\boldsymbol{\zeta} = L\,\mathbf{u}_r + \;\left(w(L) - H'\right)\;\mathbf{u}_\theta$$

where $H' = H + d_0$ (see figure 2(a)).

In the sequel, we shall derive the equations of motion for the system { shank, head } using the virtual work principle. This will yield a variational formulation of the problem. Then, an energy identity will be obtained.

In the following, we denote with the symbol $\int$ the integration over $[0, L]$ and with $\iiint$ the integration on the 3D domain occupied by the beam.

The virtual work principle states that,

$$\mathcal{P}_{\text{acc}} + \mathcal{P}_{\text{int}} = \mathcal{P}_{\text{ext}} \quad \text{where } \mathcal{P}_{\text{ext}} = \mathcal{P}_{\text{grav}} + \mathcal{P}_{\text{jack}} + \mathcal{P}_{\text{coupl,shank}} + \mathcal{P}_{\text{coupl,head}} + \mathcal{P}_{\text{string}}$$

where $\mathcal{P}_{\text{acc}}$ is the virtual work due to acceleration, $\mathcal{P}_{\text{int}}$ the virtual work due to the interior forces of the shank and $\mathcal{P}_{\text{ext}}$ the virtual work due to the exterior forces. This last item can be divided into several contributions coming from the gravity, the jack force, the coupling between the shank and the head, and the string force. The different terms are derived successively in Appendix A. Substituting them with their expression then yields a variational formulation of the problem, where A is the area of the beam section, and I is the bending moment of inertia of the beam. For instance, in the case of a circle cross-section, we have

$$A = \pi R^2 \quad \text{and} \quad I = \frac{\pi R^4}{4}, \quad \text{where } R \text{ is the radius.}$$

2.1. Variational formulation of the problem

The internal coupling force $\mathbf{F}_{\text{coupl}}$ is an unknown of the problem which has been introduced in order to treat the shank-head coupling in a mathematical weak way. The additional equation comes from imposing that the displacement of the hammer head is equal to the displacement of the extremity of the shank. This equation is called "equation of continuity shank-head".

The variational formulation directly yields from replacing the virtual works by their expression. In order to prepare for the numerical resolution, it is moreover necessary to specify the variational spaces of the solutions. Let us introduce

$$\mathcal{V}_0 = \{w \in H^1([0, L]),\ \text{such that } w(0) = 0\}.$$

One major hypothesis for writing the displacement field of the shank as equation (1) was that all exterior forces were in the $(\mathbf{u}_x, \mathbf{u}_y)$ plane. Using this hypothesis, it is straightforward to show that the solution lives in the same plane. In the following, we will only consider a 2D motion (meaning that $\boldsymbol{\xi}$ and $\mathbf{F}_{\text{coupl}} \in \mathbb{R}^2$), but for convenience we will still call $\mathbf{u}_x$, $\mathbf{u}_y$, $\mathbf{u}_r$ and $\mathbf{u}_\theta$ their projection on the 2D plane :

$$\mathbf{u}_x = \begin{bmatrix} 1 \\ 0 \end{bmatrix}, \qquad \mathbf{u}_y = \begin{bmatrix} 0 \\ 1 \end{bmatrix}, \qquad \mathbf{u}_r = \begin{bmatrix} \cos\theta \\ \sin\theta \end{bmatrix}, \qquad \mathbf{u}_\theta = \begin{bmatrix} \sin\theta \\ -\cos\theta \end{bmatrix}.$$

The reader can acquire a first intuition of the fact that an additional constraint on w is needed in order to grant the uniqueness of solutions, by realizing that several couples (θ, w) can describe a given beam position. For instance, $(\theta = 45°, w = 0)$ describes the same situation as $(\theta = 0, w(s) = -s)$, as an infinity of other couples. But, there is a unique couple which satisfies that the mean value of w is zero. Of course this criterion for the choice of a unique couple is coherent with the physical assumption for using Timoshenko theory of "small deformations". An analytical study of this criterion is beyond the scope of this article and shall be addressed in an other context. We chose to impose that the mean value of w is zero via a Lagrange multiplier technique. The Lagrange multiplier is called λ.

We seek $(w, \varphi, \theta, \lambda, \mathbf{F}_{coupl}, \boldsymbol{\xi}) \in \mathcal{V}_0 \times H^1 \times \mathbb{R} \times \mathbb{R} \times \mathbb{R}^2 \times \mathbb{R}^2$
such that for all $(w^\star, \varphi^\star) \in H^1 \times H^1$, we have

Shank equations / equation on (w, φ): (3a)

$$\int_0^L \rho A \frac{\partial^2 w}{\partial t^2} w^\star + \int_0^L AG\kappa \left(\frac{\partial w}{\partial s} - \varphi \right) \frac{\partial w^\star}{\partial s} + \lambda \int_0^L w^\star - \int \rho A \left(w\,\dot{\theta}^2 + \ddot{\theta}\, s + g\cos\theta \right) w^\star$$
$$- \left(\mathbf{F}_{coupl} \cdot u_\theta \right) w^\star(L) = -F_{jack} \int_0^L \delta_{\text{jack}}(s)\, w^\star(s)\, \mathrm{d}s$$

$$\int_0^L \rho I \frac{\partial^2 \varphi}{\partial t^2} \varphi^\star - \int_0^L AG\kappa \left(\frac{\partial w}{\partial s} - \varphi \right) \varphi^\star + \int_0^L EI \frac{\partial \varphi}{\partial s} \frac{\partial \varphi^\star}{\partial s} - \rho I \ddot{\theta} \int_0^L \varphi^\star = 0$$

Zero average of w / equation on λ: (3b)

$$\int_0^L w = 0$$

Equation on θ: (3c)

$$\ddot{\theta} \int_0^L \rho A\,(w^2 + s^2) + 2\dot{\theta} \left[\int_0^L \rho A\, w\dot{w} \right] - \int_0^L \rho A\, s\, \ddot{w} + \int_0^L \rho A\, g\ (s\cos\theta + w\sin\theta)$$
$$+ \int_0^L \rho I \left(\ddot{\theta} - \ddot{\varphi} \right) = F_{\text{jack}} \int_0^L s\delta_{\text{jack}} + (w(L) - H) \left(\mathbf{F}_{coupl} \cdot \mathbf{u}_r \right) - L \left(\mathbf{F}_{coupl} \cdot \mathbf{u}_\theta \right)$$

Head equation / equation on $\boldsymbol{\xi}$: (3d)

$$m_H\, \ddot{\boldsymbol{\xi}} = -m_H\, g\, \mathbf{u}_y - \mathbf{F}_{\text{coupl}} - F_{\text{string}}\, \mathbf{u}_y$$

Equation of continuity shank - head / equation on $\mathbf{F}_{coupl}$: (3e)

$$\boldsymbol{\xi} = L\, \mathbf{u}_r + (w(L) - H)\ \mathbf{u}_\theta$$

2.2. Energy identity

Taking as test functions $(w^\star, \varphi^\star)$ the time derivative of the unknowns (w, φ) in (3a), multiplying equation (3c) with $\dot\theta$ and multiplying equation (3d) with $\dot{\boldsymbol\xi}$ enables us to show the following energy identity:

$$\frac{\mathrm{d}\mathcal{E}}{dt} = F_{\text{jack}}\left(\dot\theta \int s\delta_{\text{jack}}(s)\,\mathrm{d}s \;-\; \int \dot w(s)\delta_{\text{jack}}(s)\,\mathrm{d}s\right) - F_{\text{string}}\,\dot{\boldsymbol\xi}\cdot\mathbf{u}_y$$

where the energy reads:

$$\mathcal{E}(t) = \frac{1}{2}\int_0^L \rho A w^2(\dot\theta)^2 + \frac{1}{2}\int_0^L \rho A(\dot w - s\,\dot\theta)^2 + \frac{1}{2}\int_0^L \rho I(\dot\theta-\dot\varphi)^2 + \frac{m_H}{2}\left|\dot{\boldsymbol\xi}\right|^2 + \frac{1}{2}\int_0^L AG\kappa\left(\frac{\partial w}{\partial s}-\varphi\right)^2 + \frac{1}{2}\int_0^L EI\left(\frac{\partial\varphi}{\partial s}\right)^2$$
$$+ \int_0^L \rho A\, g\;(s\sin\theta - w\cos\theta) + L^2\rho\,\frac{A\,g}{2} + m_H\,g\;(\boldsymbol\xi\cdot u_y) + C_g$$

Especially, this energy is preserved if exterior forces F_{jack} and F_{string} are equal to zero.

Notice that it is obtained by using the time derivative of (3e). Indeed, it allowed us to simplify the terms involving $\mathbf{F}_{\text{coupl}}$, which are nothing but internal forces to the global mechanical system.

Most terms of this energy are trivially positive. Only the last terms, associated to gravity, need a detailed explanation:

$$\begin{cases} \displaystyle\int_0^L \rho A\, g\, s\, \sin(\theta) \;+ L^2\rho A g/2 \geq 0 & \text{(4a)} \\ \displaystyle\int_0^L \rho A\, g\, w\, \cos(\theta) = 0 \quad \text{thanks to (3b)} & \text{(4b)} \end{cases}$$

The last term of the energy, $m_H\, g\, \boldsymbol\xi\cdot\mathbf{u}_y + C_g$, is not necessarily positive, but it would be with $C_g = -\sqrt{H^2+L^2}$ if the shank was not flexible (which is the macroscopic motion of the beam). Since the beam vibrations are supposed to be small, we expect that there exists a constant C_g close to its "macroscopic" equivalent that makes the contribution positive. This qualitative argument should be shown in a further analytic study which is beyond the scope of this article.

3. An energy-based numerical scheme for solving the { shank – head } system

We are guided by the desire to preserve a discrete energy, which will provide a priori estimates on the discrete solution. The energetic approach is a powerful way to later introduce couplings with other mechanical systems, in a stable and preserving way, which is our final goal in the context of the piano, beginning with the strings.

We rely on the variational form given by the set of equations (3) and perform a conformal Galerkin method in space with high order finite elements[1]. Let us denote $\mathcal{V}_{h,0} \subset \mathcal{V}_0$ and $\mathcal{V}_h \subset H^1$ the approximate spaces given as

$$[0,L] = \bigcup_k [s_k, s_{k+1}]$$
$$\mathcal{V}_h \;=\; \left\{u \in H^1([0,L]) \text{ such that } u|_{[s_k,s_{k+1}]} \in \mathbb{P}_r\right\}$$
$$\mathcal{V}_{h,0} \;=\; \{u \in \mathcal{V}_0 \text{ such that } u|_{[s_k,s_{k+1}]} \in \mathbb{P}_r\}$$

[1] for Timoshenko systems, it is known that locking phenomena can appear (see [12]), but using high order Finite Element Method diminishes this effect (see [17]).

where $\mathbb{P}_r$ is the space of polynomials of degree lower or equal to r.

Time discretisation is the main issue since it is absolutely not trivial to ensure numerical stability in such a nonlinear and coupled context, especially in view of the coupling with the rest of the instrument. Most of the terms are treated in a classical implicit way with "θ-schemes", the preserving class of Newmark schemes (see chapter XX of [10]). The weighting coefficient is chosen equal to $1/4$ in order to avoid any stability condition while maximizing the accuracy. A non classical scheme is proposed in order to discretize the inertial term. These choices lead to a stable scheme, and the over cost of implicit schemes is anyhow expected in such a nonlinear context.

We denote

$$\{X\}^n_{1/4} \;=\; \frac{X^{n+1} + 2X^n + X^{n-1}}{4} \tag{5}$$

which is a centered weighted approximation of $X(t^n)$. In the same way, we denote

$$\{\cos\theta\}^n_{1/4} := \frac{\cos\theta^{n+1} + 2\cos\theta^n + \cos\theta^{n-1}}{4} \tag{6}$$

which is a centered weighted approximation of $\cos\theta(t^n)$ where the average is done outside the cosine function. We also introduce the functions

$$\delta\cos(a,b) = \begin{cases} \dfrac{\cos a - \cos b}{a-b} & \text{if } a \neq b \\ -\sin(a) & \text{if } a = b \end{cases} \quad \text{and} \quad \delta\sin(a,b) = \begin{cases} \dfrac{\sin a - \sin b}{a-b} & \text{if } a \neq b \\ \cos(a) & \text{if } a = b \end{cases} \tag{7}$$

and finally, the oriented vectors

$$\mathbf{u}^n_r \;=\; \begin{bmatrix} \cos\theta^n \\ \sin\theta^n \end{bmatrix}, \qquad \mathbf{u}^n_\theta \;=\; \begin{bmatrix} \sin\theta^n \\ -\cos\theta^n \end{bmatrix}$$

In the sequel, numerical integration is done with quadrature techniques (see [13]) and denoted $\oint$.

3.1. Non classical treatment of the inertial term

A non-classical discretisation is done for the three contributions coming from the first term of the energy:

$$\frac{1}{2}\int_0^L \rho A\, w^2(\dot\theta)^2 \tag{8}$$

which yields the three following terms in the equations:

$$\begin{cases} -\displaystyle\int_0^L \rho A\, w\,\dot\theta^2\, w^\star & \text{for the shank's flexural equation,} \\ \ddot\theta \displaystyle\int_0^L \rho A\, w^2 + 2\dot\theta \int_0^L \rho A\, w\dot w & \text{for the equation on } \theta. \end{cases} \tag{9}$$

A first idea would be to use centered weighted approximations for w and centered quotients for the time derivatives of θ and w, but this does not lead to a conservative numerical scheme. A second idea would be to use variational time integrators methods as described in [14], but these methods do not preserve the discrete energy if the time step is constant. It is however a good starting point to find energy preserving schemes. Let us call $\mathcal{L}_h$ the discrete density of lagrangian associated to the continuous Lagrangian (8):

$$\mathcal{L}_h(q^n, q^{n+1}) = \frac{1}{2}\left(\frac{\theta^{n+1} - \theta^n}{\Delta t}\right)^2 \left(\frac{w^{n+1} + w^n}{2}\right)^2, \quad \text{where } q^n = (w^n, \theta^n) \tag{10}$$

Then the variational integration technique yields the following scheme:

$$\begin{cases} \dfrac{1}{2}\left(\dfrac{\theta^{n+1}-\theta^n}{\Delta t}\right)^2\left(\dfrac{w^{n+1}+w^n}{2}\right)+\dfrac{1}{2}\left(\dfrac{\theta^{n}-\theta^{n-1}}{\Delta t}\right)^2\left(\dfrac{w^{n}+w^{n-1}}{2}\right) & \leftarrow\ w\,\dot\theta^2 \quad (11a) \\ \dfrac{1}{\Delta t}\left(\dfrac{w^{n+1}+w^n}{2}\right)^2\left(\dfrac{\theta^{n+1}-\theta^n}{\Delta t}\right)-\dfrac{1}{\Delta t}\left(\dfrac{w^{n}+w^{n-1}}{2}\right)^2\left(\dfrac{\theta^{n}-\theta^{n-1}}{\Delta t}\right) & \leftarrow\ \ddot\theta\, w^2+2\dot\theta w\dot w \quad (11b) \end{cases}$$

This method does not preserve exactly the discrete Lagrangian $\oint_0^L \rho A\,\mathcal{L}_h$, but we use the second line of this scheme as a starting point and change the first line in order to guarantee an energy preservation. Finally, the three contributions will be discretized as follows:

$$\begin{cases} -\oint_0^L \rho A\ \dfrac{w^{n+1}+2w^n+w^{n-1}}{4}\left(\dfrac{\theta^{n+1}-\theta^n}{\Delta t}\right)\left(\dfrac{\theta^{n}-\theta^{n-1}}{\Delta t}\right)w^\star & \leftarrow\ -\displaystyle\int_0^L \rho A\, w\,\dot\theta^2\, w^\star \quad (12a) \\ \oint_0^L \dfrac{\rho A}{\Delta t}\left[\dfrac{\theta^{n+1}-\theta^n}{\Delta t}\left(\dfrac{w^{n+1}+w^n}{2}\right)^2-\dfrac{\theta^{n}-\theta^{n-1}}{\Delta t}\left(\dfrac{w^{n}+w^{n-1}}{2}\right)^2\right] & \leftarrow\ \ddot\theta\displaystyle\int_0^L \rho A\, w^2+2\dot\theta\int_0^L \rho A\, w\dot w \quad (12b) \end{cases}$$

The consistency of system (12) with the inertial terms of the equation is not straightforward and is shown in Appendix B. Since this scheme is not classical, we provide the calculations that lead to the discrete energy.

We take $w^\star = \dfrac{w^{n+1}-w^{n-1}}{2\Delta t}$ in (12a) and multiply (12b) by $\dfrac{\theta^{n+1}-\theta^{n-1}}{2\Delta t}$, and we add the contributions. We get, after denoting $w^{n+\frac12} = \dfrac{w^{n+1}+w^n}{2}$ and $\dot\theta^{n+\frac12} = \dfrac{\theta^{n+1}-\theta^n}{\Delta t}$,

$$0 = \oint_0^L -\frac{\rho A}{2\Delta t}\dot\theta^{n+\frac12}\dot\theta^{n-\frac12}\left[\left(w^{n+\frac12}\right)^2-\left(w^{n-\frac12}\right)^2\right]+\oint_0^L \frac{\rho A}{2\Delta t}\left[\left(w^{n+\frac12}\right)^2\left(\dot\theta^{n+\frac12}\right)^2+\left(w^{n+\frac12}\right)^2\dot\theta^{n+\frac12}\dot\theta^{n-\frac12}\right.$$
$$\left.-\left(w^{n-\frac12}\right)^2\left(\dot\theta^{n-\frac12}\right)^2-\left(w^{n-\frac12}\right)^2\dot\theta^{n+\frac12}\dot\theta^{n-\frac12}\right]$$

The two terms coming from (12a) both cancel with terms coming from (12b), and we get :

$$\frac{\mathcal{E}_{NL}^{n+\frac12}-\mathcal{E}_{NL}^{n-\frac12}}{\Delta t}=0, \quad \text{where } \mathcal{E}_{NL}^{n+\frac12}=\oint_0^L \frac{\rho A}{2}\left(\frac{\theta^{n+1}-\theta^n}{\Delta t}\right)^2\left(\frac{w^{n+1}+w^n}{2}\right)^2$$

3.2. Numerical scheme

The numerical scheme that we propose, based on our innovative treatment of the inertial terms, is the following:

$$
\left\{
\begin{array}{l}
\text{We seek } (w^{n+1}, \varphi^{n+1}, \theta^{n+1}, \lambda, \mathbf{F}_{coupl}, \boldsymbol{\xi}^{n+1}) \in \mathcal{V}_{h,0} \times \mathcal{V}_h \times \mathbb{R} \times \mathbb{R}^2 \times \mathbb{R}^2 \\
\qquad\qquad \text{such that for all } (w^\star, \varphi^\star) \in \mathcal{V}_{h,0} \times \mathcal{V}_h, \text{ we have} \\
\textbf{Shank equations:} \qquad (13a) \\
\displaystyle\oint_0^L \rho A \frac{w^{n+1} - 2w^n + w^{n-1}}{\Delta t^2} w^\star + \oint_0^L AG\kappa \left\{ \frac{\partial w}{\partial s} - \varphi \right\}_{1/4}^n \frac{\partial w^\star}{\partial s} + \lambda \oint_0^L w^\star \\
\displaystyle - \oint \rho A \left[\frac{w^{n+1} + 2w^n + w^{n-1}}{4} \left(\frac{\theta^{n+1} - \theta^n}{\Delta t} \right) \left(\frac{\theta^n - \theta^{n-1}}{\Delta t} \right) + \frac{\theta^{n+1} - 2\theta^n + \theta^{n-1}}{\Delta t^2} s + g \left\{ \cos\theta \right\}_{1/4}^n \right] w^\star \\
\displaystyle - \left(\mathbf{F}_{\text{coupl}} \cdot \mathbf{u}_\theta^n \right) w^\star(L) = -F_{\text{jack}} \oint_0^L \delta_{\text{jack}}(s) w^\star(s)\, \mathrm{d}s \\
\displaystyle\oint_0^L \rho I \frac{\varphi^{n+1} - 2\varphi^n + \varphi^{n-1}}{\Delta t^2} \varphi^\star - \oint_0^L AG\kappa \left\{ \frac{\partial w}{\partial s} - \varphi \right\}_{1/4}^n \varphi^\star + \oint_0^L EI \left\{ \frac{\partial \varphi}{\partial s} \right\}_{1/4}^n \frac{\partial \varphi^\star}{\partial s} \\
\displaystyle - \rho I \frac{\theta^{n+1} - 2\theta^n + \theta^{n-1}}{\Delta t^2} \oint_0^L \varphi^\star = 0 \\
\textbf{Zero average of } w\textbf{:} \qquad (13b) \\
\displaystyle\int_0^L \{w\}_{1/4}^n = 0 \\
\textbf{Equation on } \theta\textbf{:} \qquad (13c) \\
\displaystyle\frac{\theta^{n+1} - 2\theta^n + \theta^{n-1}}{\Delta t^2} \oint_0^L \rho A\, s^2 + \oint_0^L \frac{\rho A}{\Delta t} \left[\frac{\theta^{n+1} - \theta^n}{\Delta t} \left(\frac{w^{n+1} + w^n}{2} \right)^2 - \frac{\theta^n - \theta^{n-1}}{\Delta t} \left(\frac{w^n + w^{n-1}}{2} \right)^2 \right] \\
\displaystyle + \oint_0^L \rho A\, g \left[s\, \delta \sin(\theta^{n+1}, \theta^{n-1}) - \{w\}_{1/4}^n\ \delta \cos(\theta^{n+1}, \theta^{n-1}) \right] \\
\displaystyle - \oint_0^L \rho A\, s \frac{w^{n+1} - 2w^n + w^{n-1}}{\Delta t^2} + \oint_0^L \rho I \left[\frac{\theta^{n+1} - 2\theta^n + \theta^{n-1}}{\Delta t^2} - \frac{\varphi^{n+1} - 2\varphi^n + \varphi^{n-1}}{\Delta t^2} \right] \\
\displaystyle = F_{\text{jack}} \oint_0^L s\delta_{\text{jack}} + \left(\{w\}_{1/4}^n\ (L) - H \right) \left(\mathbf{F}_{\text{coupl}} \cdot \mathbf{u}_r^n \right) - L \left(\mathbf{F}_{\text{coupl}} \cdot \mathbf{u}_\theta^n \right) \\
\textbf{Head equation:} \qquad (13d) \\
\displaystyle m_H \frac{\boldsymbol{\xi}^{n+1} - 2\boldsymbol{\xi}^n + \boldsymbol{\xi}^{n-1}}{\Delta t^2} = -m_H\, g\, \mathbf{u}_y - \mathbf{F}_{\text{coupl}} - F_{\text{string}}\, \mathbf{u}_y \\
\textbf{Equation of continuity shank - head:} \qquad (13e) \\
\displaystyle\frac{\boldsymbol{\xi}^{n+1} - \boldsymbol{\xi}^{n-1}}{2\Delta t} = \frac{\theta^{n+1} - \theta^{n-1}}{2\Delta t} \left[\{w\}_{1/4}^n\ (L) - H \right] \mathbf{u}_r^n + \left[\frac{w^{n+1} - w^{n-1}}{2\Delta t}(L) - L \frac{\theta^{n+1} - \theta^{n-1}}{2\Delta t} \right] \mathbf{u}_\theta^n
\end{array}
\right.
$$

Notice that the equations of continuity are consistent with the time derivative of conditions (3e). This will enable us to show a discrete energy preservation.

3.3. Discrete energy

A discrete energy identity can be obtained by following the classical steps:

- taking in (13a) as test functions : $w^\star = \dfrac{w^{n+1} - w^{n-1}}{2\Delta t}$, $\varphi^\star = \dfrac{\varphi^{n+1} - \varphi^{n-1}}{2\Delta t}$,
- multiplying (13c) by $\dfrac{\theta^{n+1} - \theta^{n-1}}{2\Delta t}$,
- multiplying (13d) by $\dfrac{\boldsymbol{\xi}^{n+1} - \boldsymbol{\xi}^{n-1}}{2\Delta t}$.

Notice that by definition,

$$\delta\ \sin(\theta^{n+1}, \theta^{n-1})\left(\theta^{n+1} - \theta^{n-1}\right) = \cos(\theta^{n+1}) - \cos(\theta^{n-1}) \ \text{ and } \ \delta\ \cos(\theta^{n+1}, \theta^{n-1})\left(\theta^{n+1} - \theta^{n-1}\right) = \sin(\theta^{n+1}) - \sin(\theta^{n-1}).$$

The interior coupling terms will vanish thanks to equation (13e).

Without any source term ($F_{\text{jack}} = F_{\text{string}} = 0$), the following discrete energy is preserved from one time step to the following:

$$\mathcal{E}^{n+\frac{1}{2}} = \mathcal{E}_{\text{kin}}^{n+\frac{1}{2}} + \mathcal{E}_{\text{pot}}^{n+\frac{1}{2}}, \text{ where} \tag{14}$$

$$\mathcal{E}_{\text{kin}}^{n+\frac{1}{2}} = \frac{1}{2}\oint_0^L \rho A \left(\frac{\theta^{n+1} - \theta^n}{\Delta t}\right)^2 \left(\frac{w^{n+1} + w^n}{2}\right)^2 + \frac{1}{2}\oint_0^L \rho A \left[\frac{w^{n+1} - w^n}{2\Delta t} - s\frac{\theta^{n+1} - \theta^n}{2\Delta t}\right]^2 + \frac{1}{2}\oint_0^L \rho I \left[\frac{\theta^{n+1} - \theta^n}{\Delta t} - \frac{\varphi^{n+1} - \varphi^n}{\Delta t}\right]^2 + \frac{m_H}{2}\left|\frac{\boldsymbol{\xi}^{n+1} - \boldsymbol{\xi}^n}{\Delta t}\right|^2 \tag{15}$$

$$\mathcal{E}_{\text{pot}}^{n+\frac{1}{2}} = \frac{1}{2}\oint_0^L AG\kappa \left[\frac{\partial}{\partial s}\left(\frac{w^{n+1} + w^n}{2}\right) - \frac{\varphi^{n+1} + \varphi^n}{2}\right]^2 + \frac{1}{2}\oint_0^L EI\left[\frac{\partial}{\partial s}\left(\frac{\varphi^{n+1} + \varphi^n}{2}\right)\right]^2 + \oint_0^L \rho A\, g\, s\, \frac{\sin\theta^{n+1} + \sin\theta^n}{2} + L^2\rho A g/2 - \oint_0^L \rho A\, g\, \frac{w^{n+1} + w^n}{2}\frac{\cos\theta^{n+1} + \cos\theta^n}{2} + m_H\, g\, \frac{\boldsymbol{\xi}^{n+1} + \boldsymbol{\xi}^n}{2} \cdot u_y + C_g \tag{16}$$

Using classical tools (see [15]), the positivity of this quantity would grant the unconditional stability of the numerical scheme. As in the continuous case, we have:

$$\begin{cases} \displaystyle\oint_0^L \rho A\, g\, s\, \frac{\sin\theta^{n+1} + \sin\theta^n}{2} + L^2\rho A g/2 & \geq 0 \\ \displaystyle\oint_0^L \rho A\, g\, \frac{w^{n+1} + w^n}{2}\frac{\cos\theta^{n+1} + \cos\theta^n}{2} & = 0 \quad \text{thanks to (13b), and assuming that } \displaystyle\oint_0^L w^0 = \oint_0^L w^1 = 0. \end{cases}$$

The only terms which are not necessarily positive is $m_H\, g\, \dfrac{\boldsymbol{\xi}^{n+1} + \boldsymbol{\xi}^n}{2} \cdot \mathbf{u}_y + C_g$, as in the continuous case. The same qualitative argument applies, therefore this term is expected to be positive.

4. Numerical simulations and prospects

For the numerical simulations that follow, the hammer shank and head are coupled to one or several vibrating strings, which are coupled to a soundboard that radiates in the air, as in a real piano. Therefore, in the following, F_{string} is not longer a given force, but comes from the interaction between the hammer head and the string(s), which is (are) now free to vibrate. At the origin of times, the piano action is at rest, meaning that $\theta \approx -17$ deg. The strings are at rest and occupy the horizontal line $y = H + d_0$ (see figure 2(a)) so that, macroscopically, the hammer head - string contact begins when the angle θ is equal to 0. This choice was motivated by several observations in real pianos, but is not universally respected in the instrument manufacture. The hammer head - string contact is treated as in [8] which means that strong hypotheses have been made :

- the contact region on the string is a fixed interval of the string,
- the interacting force is a nonlinear function of the distance d between the hammer head and the string, with hysteresis. This nonlinear function F_{string} is defined as (see [8])

$$F_{\text{string}}(d) = K\,\Phi(d) + R\,\frac{\mathrm{d}}{\mathrm{d}t}\Phi(d), \qquad \Phi(d) = \left[(d_0 - d)^+\right]^p \tag{18}$$

  where p is a positive real number, d_0 is the distance between ξ and the top of the hammer head ζ at rest (see figure 2(a)), and $(\cdot)^+$ stands for the positive part.

In the model described in reference [8], the hammer head was only allowed a vertical motion, whereas in the present shank model an horizontal motion of the hammer head can occur. However, for the following numerical results, the distance d has been defined as the *vertical* distance between the hammer head and the string. This means that only the vertical position of the hammer head counts in the contact. This is a rough description of the geometry and we will discuss a possible improved model in section 4.4.

A new feature that we had to model was the let-off mechanism. In real pianos, the jack (see figure 1) pushes the shank until the jack's other end touches a fixed obstacle which makes it rock and loose contact with the shank. In a first approach, we modeled this mechanism as the following : as soon as the distance between the hammer head and the string (at rest) is smaller than the so-called *let-off distance*, the jack force is set to zero. In a real piano, the contact element between the jack and the shank (the roller) is covered with felt, and therefore the contact loss is probably smoother. In the absence of experimental data concerning this felt and its crushing law, we chose this abrupt solution but a better model could be implemented in the future.

The modeling of the strings, soundboard and air is beyond the scope of this article, so we refer the reader to [8] for a description of the mechanical model of the whole piano with stiff and nonlinear vibrating strings, and to [15] and [19] for a description of the innovative energy preserving numerical schemes used to solve the equations. The coupling between the numerical scheme (13) and the numerical scheme done on the strings and the rest of the piano is handled via Lagrange multipliers which are the coupling forces F_{string} (one for each string).

The numerical experiments are conducted with the shank's parameters given in table 4 (taken from [6]) and the head's parameters given in table 4. The piano's parameters can be retrieved in [18].

L (m)	E (Pa)	A (m^2)	ρ ($\text{kg}\cdot\text{m}^{-3}$)	I (m^4)	G (Pa)	κ (-)
0.086	$10.18 \cdot 10^9$	$32.38 \cdot 10^{-6}$	560	$83.44 \cdot 10^{-12}$	$0.64 \cdot 10^9$	0.85

Table 1: Shank parameters

H (m)	d_0 (m)	m_H (kg) :	for D♯1	for C♯5
0.04	0.02		$10.76 \cdot 10^{-3}$	$7.90 \cdot 10^{-3}$

Table 2: Heads parameters

The jack force F_{jack} is applied around a point located 0.0155 m from the rotation center of the shank (point $(0, 0)$ in figure 2(a)). The repartition function δ_{jack} stands for the roller's width. The time dependency of the jack force is a data of our simulations that we need to provide. In the literature, no experimental data of grand piano jack-shank forces

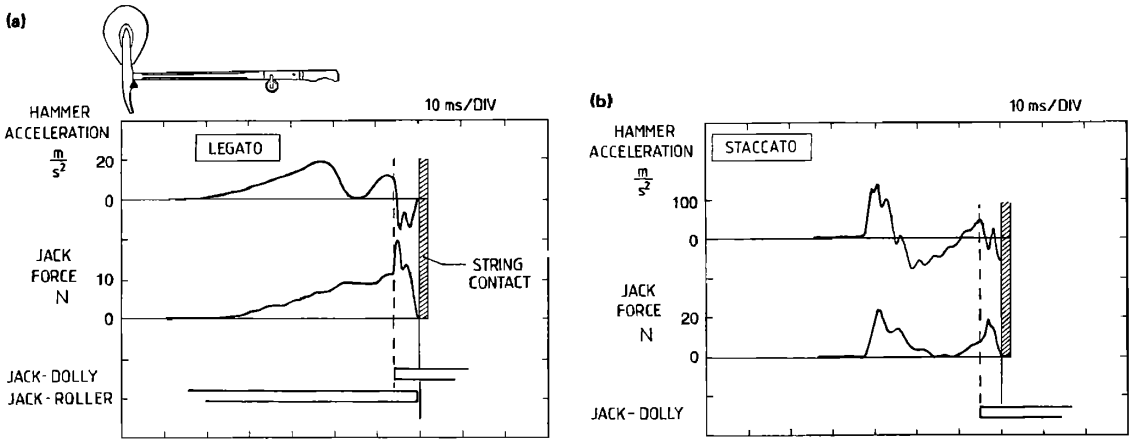

(a) Legato touch

(b) Staccato touch

Figure 3: "Registration of acceleration at the hammer head and compression force in the jack (*mezzo forte*, C_4). The force was measured by means of a piezofoil in the jack. The position of the accelerometer is marked with a triangle. Also shown are the contacts signals jack dolly and jack roller. (a) Legato touch and (b) Staccato touch." Figure taken from [3].

and hammer - string interaction forces are exploitable, partly because they seem difficult to achieve with precision and/or because of unjustified assumptions in the experimental setup (see [5]). However, two examples of jack-shank forces can be found in [3] as reproduced in figure 3. From this figure, we have isolated two kinds of piano touches, trying to mimic the so-identified *legato* and *staccato* touches. The *staccato* touch will be associated with a strong and short pulse as a jack force, returning to zero before any let-off mechanism. The *legato* touch will be associated with an increasing jack force which only stops because of the presence of a let-off mechanism. Both touches will be modeled with the following formula for F_{jack}, only changing the parameters t_{jack} and A_{jack}.

$$F_{\text{jack}}(t) = \begin{cases} A_{\text{jack}} \cos^2\left(\dfrac{\pi}{2}\left(\dfrac{2\,t}{t_{\text{jack}}} - 1\right)\right), & \text{if } 0 \le t \le t_{\text{jack}} \\ 0, \quad \text{otherwise} \end{cases} \tag{19}$$

Once again, this is only a rough modeling of a very complex situation, which could be improved in the future.

The purpose of the following numerical simulations is first to numerically demonstrate the preservation of a discrete energy (see 4.1), and more interestingly, to illustrate the versatility of our simulation tool. The nonlinear system that we modeled and solved in this article depends on several physical parameters which are very interesting to explore. We will first investigate the effect of the pianistic touch via the jack force (see 4.2), and of the let-off distance (see 4.3). During these investigations, we will discuss the possible presence of a "longitudinal touch precursor" (see 4.4) in the piano sound.

4.1. Numerical algorithm and energy preservation

The nonlinear system (13) is solved with a modified Newton-Raphson method. The jacobian matrix is manually implemented and is only recomputed if the Newton iteration procedure does not lead to a satisfying solution. In order to decrease memory storage and the number of equations to solve, the degrees of freedom corresponding to the hammer and the shank as well as the corresponding equations are removed from the computation when the coupling force between the hammer head and the strings returns to zero for a long time.

In this paragraph, we only consider the hammer shank, head and piano strings. When the damping terms (included in the string, and in the hammer - string interaction) are set to zero, the global discrete energy of the { string, shank,

head } system is conserved as shown in figure 4. This figure was obtained for note C♯5 (the hammer strikes 3 strings, see [18] for more details on the parameters) which is the 53^{rd} key of a regular keyboard, using a constant jack force until let-off. The let-off distance was 3 mm for this simulation.

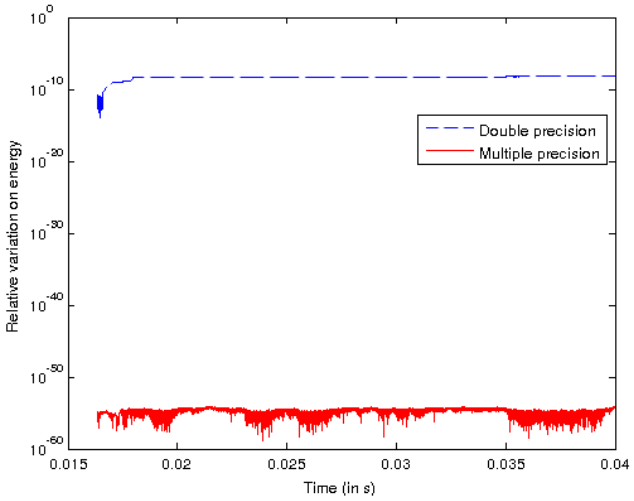

Figure 4: Relative error on the energy versus time after let-off. Double precision ($\varepsilon = 2 \cdot 10^{-16}$) and multiple precision ($\varepsilon = 10^{-60}$) are compared.

When arithmetic with multiple precision is used for the numerical computations with a precision equal to 10^{-60}, the energy seems to be very well conserved, confirming that the employed numerical method is conservative and stable. However, it can be observed some loss of accuracy, since the relative error on the energy is around 10^{-54}. In double precision (the precision being equal to $2 \cdot 10^{-16}$), the relative error is approximately equal to 10^{-8}. We think that an adimensionalization procedure should reduce this loss of accuracy.

4.2. Influence of pianistic touch

Our simulation tool enables us to study the influence of various parameters on the whole mechanical system. One of the most interesting parameters is the way the pianist strikes the key, also called "pianistic touch". As said earlier, the jack force is a data to our model, but it is only an intermediate force in the whole piano mechanism. Very few experimental recordings of this force are available and trustworthy (see [5]), so we chose to use formula (19) to represent the jack force. Moreover, we recall that the let-off mechanism is abruptly represented by the fact that this force is set to zero when the distance between the hammer head and the string becomes smaller than the let-off distance. The following results are obtained with note D♯1 which only has one string (see [18] for more details on the parameters).

In the following, we will compare two simulations coming from the jack forces obtained with the parameters **S** and **L** listed in table 3. These two simulations have very different jack forces but the hammer head hits the string at about the same velocity (around 3.4 m/s), so that only the pianistic touch differs. They will schematically stand for staccato and legato touches, this classification will come from the comparison with the experimental measurements of figure 3.

Figure 5 shows different quantities obtained by simulation of note D♯1, using parameters **S** (left) and **L** (right) of table 3. In the upper frame **S** is displayed a global view of the string (length 1.965 m) and the hammer (shank and head). In the six frames (a) to (f) are displayed the shank and head deformations at different instants, in regular scale (black) and magnified scale (blue). In frames **J** and **F** are respectively displayed the jack force and the hammer - string interaction force with respect to time. The magnified shank deformation is clearly visible before the hammer - string

Parameters set	t_{jack} (s)	A_{jack} (N)	let-off distance (m)
S	0.007	70	0.0015
L	0.100	30	0.0015
L+	0.100	30	0.0030
L-	0.100	30	0

Table 3: Parameters of jack forces for different simulations

contact (see frame (a) of figure 5(a)) but also during hammer - string contact (frames (c), (d) and (e) of figure 5(a) and 5(b)). The maximum time in frames **J** and **F** is different (25 ms for figure 5(a) and 45 ms for figure 5(b)) because the hammer does not reach the string at the same moment for both jack forces. The jack force obtained with parameters **S** of table 3 is very short and strong, while the jack force obtained with parameters **L** is progressively increasing. As a result, the jack force **S** is like a *flick* for the hammer shank, which is let free to move very soon (when the jack force returns to zero). On the contrary, the jack force **L** is still increasing when the shank reaches the let-off point, and therefore is suddenly set to zero because of this let-off mechanism. Comparing to figure 3 leads us to classify the jack force **S** as a *staccato* touch, and the jack force **L** as a *legato* touch.

This work was initially motivated by discrepancies between our experimental measurements and our simulated results. In the following, we will try to assess to what extent our new hammer shank - head model can diminish these dissimilarities, and evaluate the impact of the pianistic touch on the sound, if any.

Whereas it is very difficult to measure a jack force, it is rather easy to measure the shank acceleration. Putting a small accelerometer at the end of the shank enabled us to measure it on a Steinway D grand piano (see [8] for more details and figure 6(b) for a photography of the experimental setup). For note D♯1 struck *ff* (very strong attack), we obtained the experimental signal plotted in figure 6(b). In article [8], we noticed some "additional small oscillations" in the hammer acceleration which did not appear on the simulated hammer acceleration. At the time, no hammer shank was included in our piano model, the hammer was only represented by a hammer head given an initial velocity towards the strings, without accounting for gravity. We therefore made the hypothesis that these oscillations were due to the vibrations of the hammer shank. In figure 6(a), we have plotted the hammer head acceleration in the direction u_θ, so that it can be directly compared to the experimental signal. The acceleration obtained with a *legato* touch is in blue and the acceleration obtained with a *staccato* touch is in red. As a reference, we have put on the same graph, in black, the hammer head acceleration obtained using the old model described in [8], without any shank nor gravity, setting the initial hammer velocity close to the hammer head - string contact velocity of the other two simulations : $v_0 = 3.41$ m/s. A first remark is that both *legato* and *staccato* accelerations exhibit oscillations that the acceleration obtained with no shank does not. The acceleration simulated with the *legato* touch shows very fast oscillations which appear after let-off, because of the discontinuity created by this mechanism. These oscillations are very similar to the ones of the experimental signal, showing that **accounting for the shank in the hammer - string interaction can explain the presence of strong oscillations in the hammer head acceleration**. However, the simulated acceleration is clearly oscillating too much with the *legato* touch, most likely because our model of let-off is too abrupt compared to what happens in a real piano mechanism. A better model should account for the un-crushing of the roller felt (element of contact between the jack and the hammer shank), which is expected to make the jack force smoother during let-off. A second remark is that different pianistic touches will lead to very different hammer head acceleration signals. An interesting question is to know whether this difference is noticeable as well in the hammer head - string interaction force, since this is the only transmitted quantity to the rest of the piano structure, and ultimately, the sound.

In figure 7 are displayed the hammer head - string interaction forces for *legato* and *staccato* touches (in blue and red)

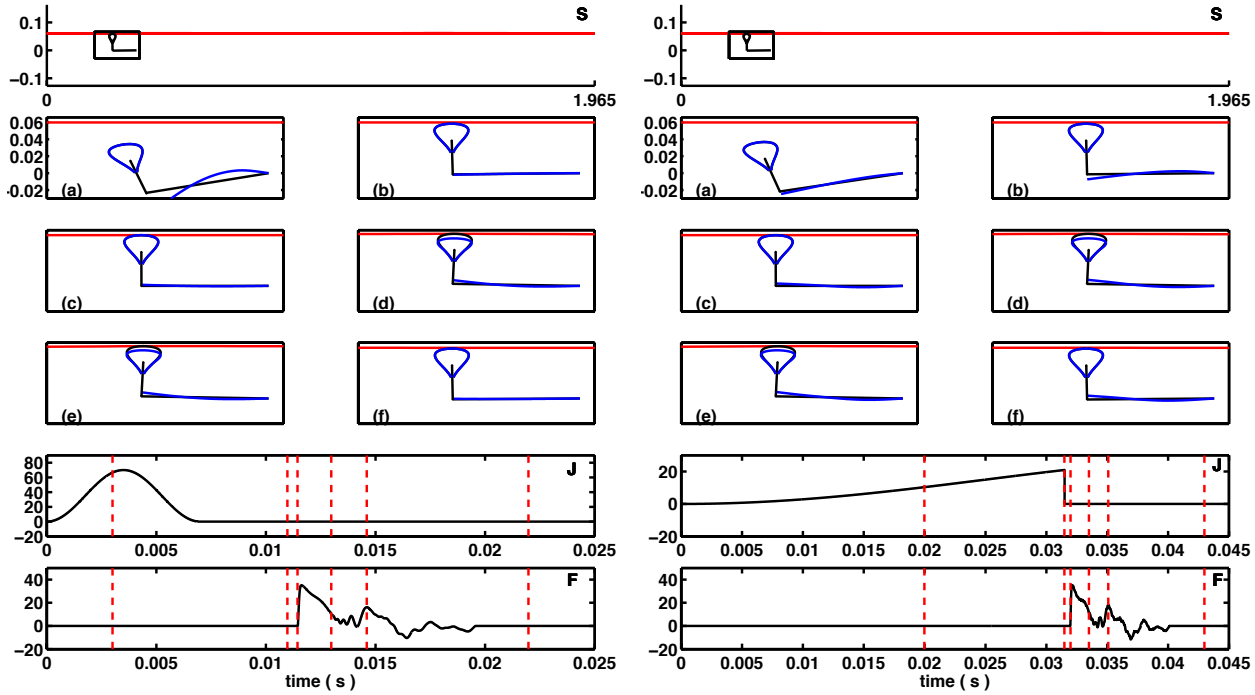

(a) Staccato touch

(b) Legato touch

Figure 5: Visualization of shank vibrations and hammer crushing after pianistic attack for *staccato* (left) and *legato* (right) touches. Frame **S** shows the whole string and the hammer at the same scale. The black rectangle is zoomed in at several times in frames (a) to (f). (a) : during jack force increase. (b) : at let-off distance. (c) : at hammer head - string contact. (d) : during the first decrease of the interaction force. (e) : at a second maximum of the interaction force. (f) : after hammer - string contact. Shank vibrations are magnified 30 times (in blue) and hammer crushing is magnified 7 times (in blue). Frames **J** and **F** respectively show the jack force and the interaction force with respect to time. The red vertical dashed lines correspond to the instants of frames (a) to (f).

and with no shank (in black) with respect to time (figure 7(a)) and with respect to frequency (figure 7(b)). The three forces clearly differ in the time domain, but more spectacularly in the frequency domain, especially around 600 Hz where the *staccato* force exhibits a drop in its spectrum of 10 dB compared to the spectrum of the force obtained with no shank, and the *legato* force exhibits a drop even more dramatic of about 25 dB. The precise physical reason for this drop is still to understand.

Simulations of the global piano model described in [8] coupled with our new hammer model make it possible to compare the sound pressure signals obtained for these pianistic touches, and with no shank. Results are displayed in figure 8, where the first subfigure is obtained for a *legato* touch, the second one with a *staccato* touch and the last one with no shank. As expected, the observations made on the spectrum of the interaction forces are clearly visible in the sound pressure spectrum. The partials 14 to 19 are present at very different levels from one touch to the other. For instance, partial 16 is below -40 dB for the *legato* touch (let-off distance of 1.5 mm), but reaches almost -20 db in the *staccato* touch, and is above -20 dB when no shank is simulated. These discrepancies are audible in the isolated sounds for a trained ear, and the authors believe that they certainly induce a sound "color" when present in a musical phrase. Moreover, the touch seems to influence the levels of the longitudinal harmonics (these harmonics are responsible for the "bell" like color of bass piano sounds, and come from the propagation of waves in the elongation direction of the string): for this string, the fundamental frequency of the longitudinal wave is equal to 550 Hz. Its second harmonic, around 1100 Hz, and indicated by $2\,f_L$ in the figures, is clearly visible, audible, and at different levels from one pianistic touch to the other (-26.3 dB for the *legato* touch and -18.8 dB for the *staccato* touch). To sum up, it is clear from these numerical experiments where all parameters, touch excepted, are rigorously the same,

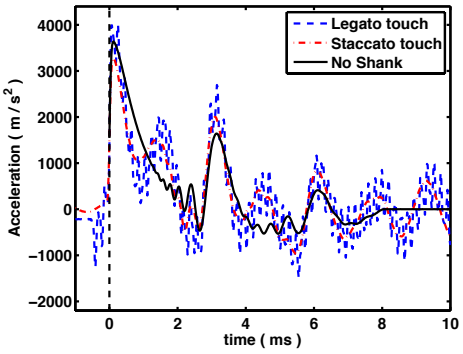

(a) Simulated accelerations

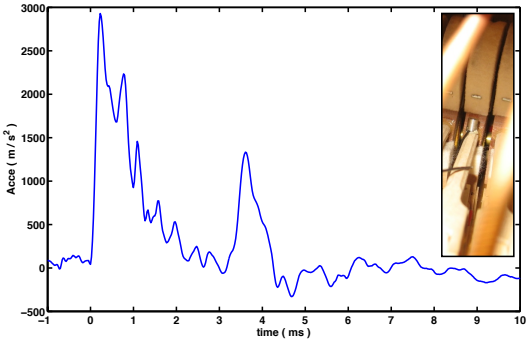

(b) Experimental acceleration and photography of the accelerometer fixed on the shank

Figure 6: Comparison between simulated (left) and experimental (right) acceleration of the hammer head. The time scale has been shifted so that time 0 corresponds to the contact instant between the hammer head and the string.

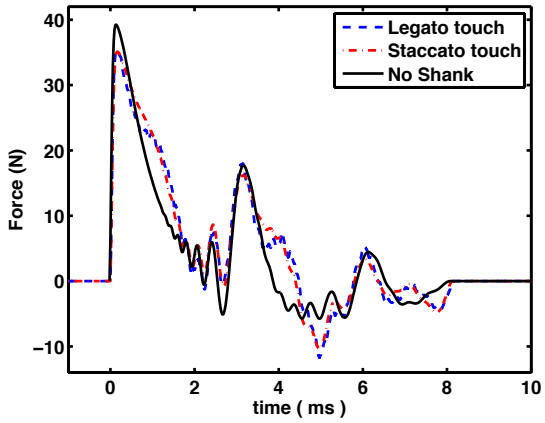

(a) Hammer string interaction forces

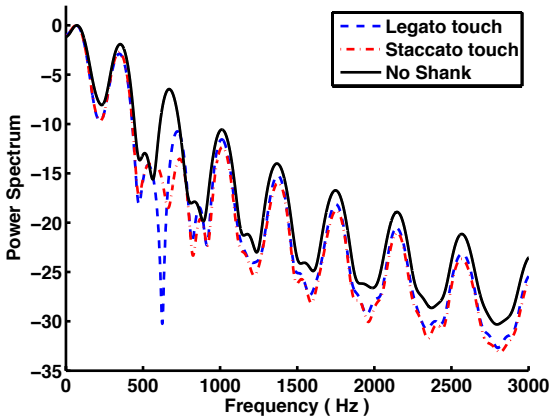

(b) Power spectrum of the interaction forces

Figure 7: Temporal and spectral profiles of hammer head - string interaction forces obtained with different pianistic touches. The time scale has been shifted so that time 0 corresponds to the contact instant between the hammer head and the string.

that **the pianistic touch can remarkably influence the piano sound color.** Notice that these spectral discrepancies only come from the differences in hammer shank vibrations. Indeed, they cannot come from other suggested causes in the literature as a shock excitation on the structure, nor from a changing impact point, nor a "longitudinal rubbing motion" on the string, since neither of these features are modeled in our study. The shock excitation on the structure measured in [1, 2] is clearly associated to real *staccato* touches and its effects add up to the spectral change that we highlighted here thanks to our simulation tool.

4.3. Influence of the let-off distance

Another very interesting parameter to explore with our simulation tool is the let-off distance. This distance is a note by note setting done by the piano technician. We recall that in our model, as soon as the distance between the hammer head and the string (at rest) is smaller than the let-off distance, the jack force is set to zero. This is a crude modeling of reality but allows us to draw qualitative conclusions. Since the let-off distance is not relevant when using a *staccato* touch (because the force is already zero when the hammer head reaches the let-off point), the following tests have been made with three different let-off distances using a *legato* touch (simulations **L**, **L+** and **L-** of table 3). Very extreme let-off distances have been tested : 3.0 mm, 1.5 mm as in the previous paragraph, and 0.0 mm, meaning that the jack

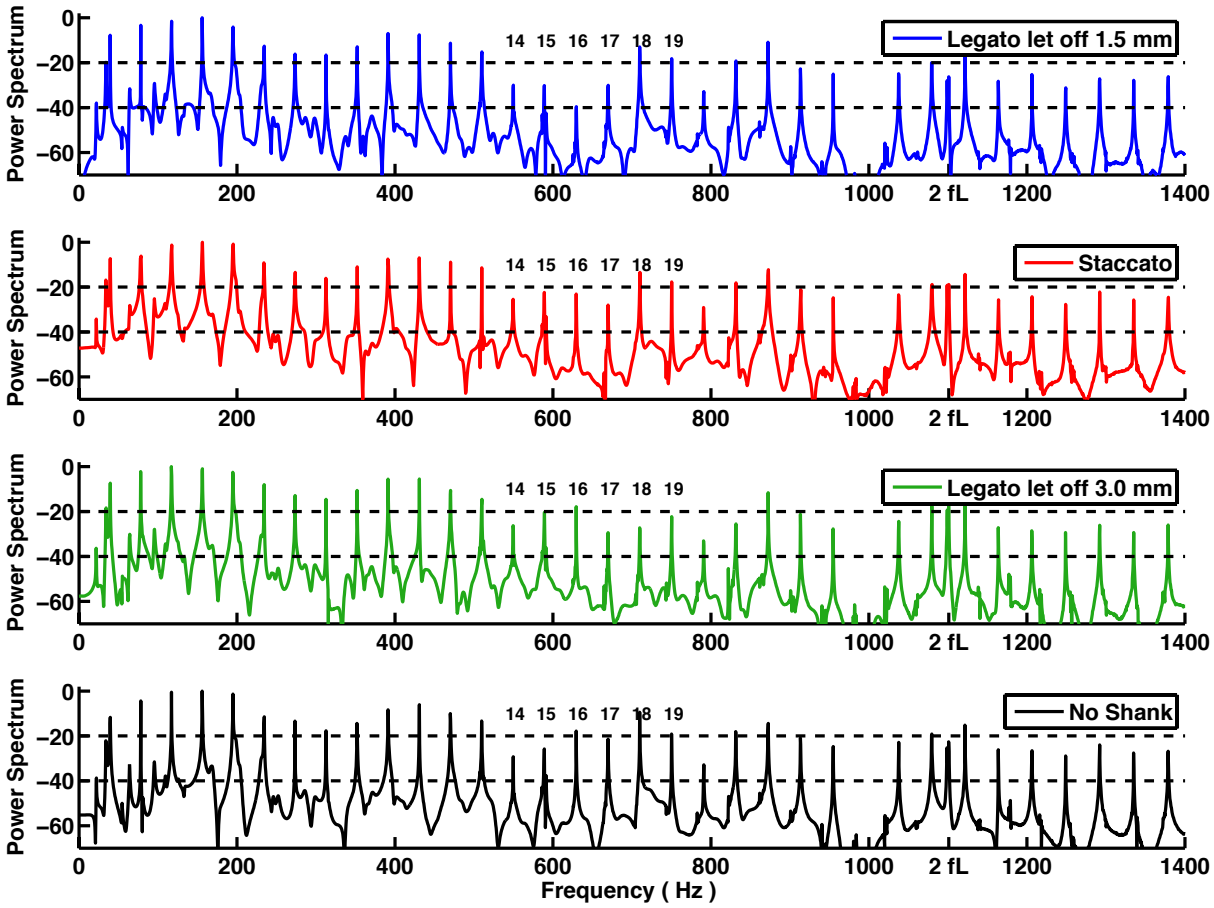

Figure 8: Spectral profiles between 0 and 1400 Hz of the sound pressure at point $x = 0.850$, $y = 1.459$, $z = 0.380$, in a cartesian coordinate system in which the soundboard is in the plane $z = 0.200$. Y-scales are in decibel (logarithmic) and normalized. Black dashed lines indicate the −20 dB and −40 dB levels in all the figures, for easy comparison.

force is set to zero at the exact contact time between the hammer head and the string. Interaction forces are displayed in figure 9 with respect to time (figure 9(a)) and with respect to frequency (figure 9(b)). **There is a clear influence of the let-off distance on the interaction force, hence on the resulted sound**. The difference on the force is rather spectacular in the [500 − 1000] Hz region of the spectrum, with discrepancies up to 20 dB in very audible zones. The influence of the let-off distance on the resulted piano sound can be observed in figure 8, where the first subfigure is obtained for simulation **L** and the third one for simulation **L+**. The partials 14 to 19 are present at very different levels (see for instance partial 16 : 20 dB different), which has a great influence on the timbre.

4.4. Pianistic touch longitudinal precursor

In real piano mechanisms, the hammer head can have a planar motion (as opposed to a vertical motion only, in the model of article [8]). Of course the main contribution of the hammer on the string is a vertical impulse, but there might exist a horizontal impulse coming from a rubbing motion of the hammer head on the string, as suggested in [3]. In our model, we have not considered this interaction, the system behaves as if the string was very *slippery* : the hammer head is free to have any horizontal motion, with no influence on the string. However, we can quantify this motion in order to estimate its extent on the resulted sound. To do so, two quantities are computed :

$$v_\theta = \frac{\mathrm{d}\xi}{\mathrm{d}t} \cdot \mathbf{u}_\theta \qquad \text{and} \qquad v_r = \frac{\mathrm{d}\xi}{\mathrm{d}t} \cdot \mathbf{u}_r$$

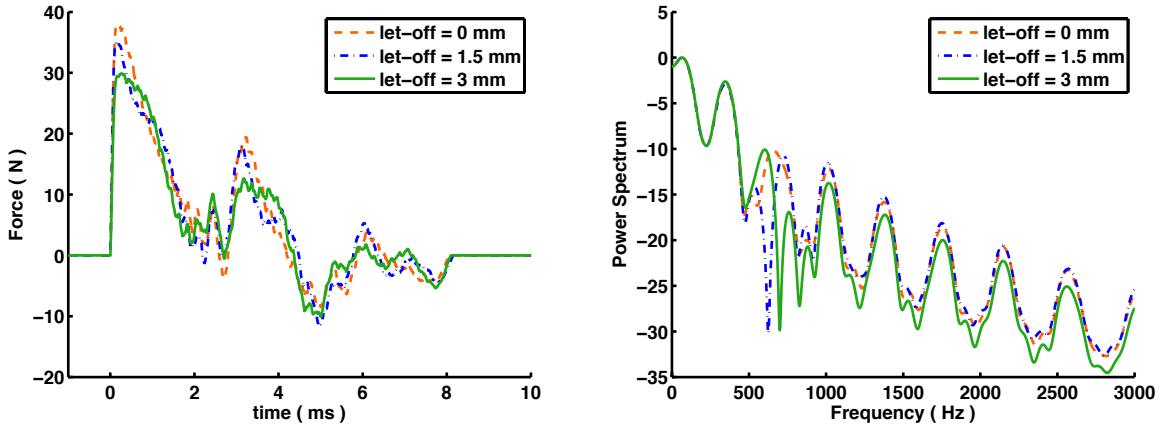

(a) Hammer string interaction forces

(b) Power spectrum of the interaction forces

Figure 9: Interaction forces obtained with different let off distances (*legato* touch). The time scale has been shifted so that time 0 corresponds to the contact instant between the hammer head and the string.

When the hammer and the string are in contact, the macroscopic angle θ is very small, thus v_θ and v_r can be interpreted as vertical and horizontal velocities. The vertical and horizontal velocities for *legato* and *staccato* touches are respectively displayed in figure 10(a) and 10(b) with respect to time. A first remark is that the horizontal velocity during contact (from 0 to 8 ms) is not small at all and oscillated between -1.5 and 1 m/s, which corroborates the hypothesis of a possible rubbing motion of the hammer head on the string. Another remark is that this horizontal velocity is quite different from one touch to the other, which leads us to believe that **accounting for this rubbing motion could help us explain the influence of the pianistic touch in the piano sound.**

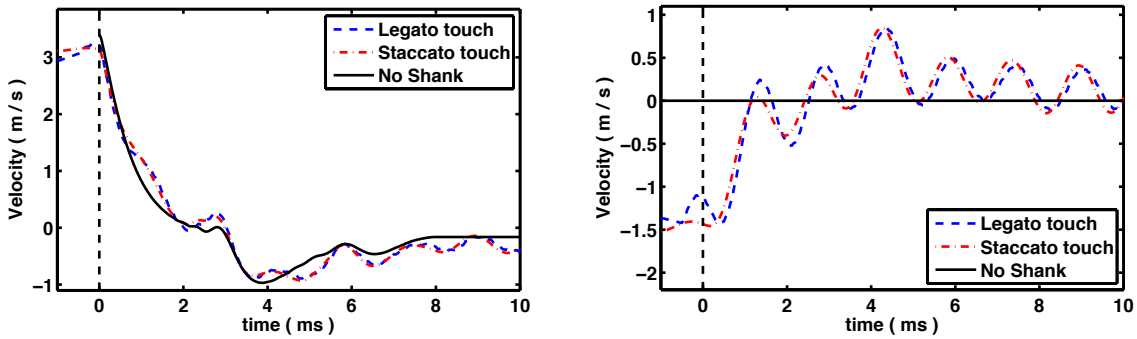

(a) Vertical velocity

(b) Horizontal velocity

Figure 10: Velocity of the hammer head for Legato and Staccato touches. The time scale has been shifted so that time 0 corresponds to the contact instant between the hammer head and the string.

A first approach in order to model this rubbing motion would be to implement a continuity displacement relation in the horizontal direction between the hammer head and the string, as if they were not allowed to slip horizontally. The equations would have to respect an energy identity in order to be included in our model. Of course if such an interaction occurred, the hammer head would probably move less than what we can see in figure 10(b) where the horizontal motion is totally free. In such a model, the string would therefore be given an impulse in its elongation direction, making a "longitudinal" wave propagate in the string. The string model that we considered in [8] already accounted

for the presence of longitudinal waves (see figure 11(a)) because of their importance, via a nonlinear coupling with the transversal waves, in the generation of specific partials in the spectrum (so called "phantom partials") and in the presence of a nonlinear precursor in the time domain. This new model of rubbing would be a new way of generating longitudinal waves in the piano string that should significantly enrich the piano model and allow us to highlight the presence of a **new precursor coming from the pianistic touch**, and confirm the experimental intuition of [3]. Furthermore, this "pianistic touch longitudinal precursor" would certainly present a greater amplitude compared to the nonlinear precursor, which is only a second order phenomenon (see [19]) and would add up the one coming from the shock on the structure.

When the shank is modeled as a flexible beam, the hammer head - string contact point is not necessarily the top of the hammer head, because a rotation of the hammer head can occur, due to the bending of the hammer shank. Another improvement of the model related to the presence of a horizontal motion of the hammer head, would therefore be to compute the interaction force of equation (18) :

- with the real distance d between the hammer head and the string (no longer projected on the vertical axis),
- with coefficients p, K, and R that depend on the impact zone of the hammer head.

The first point is rather straightforward once noticed that the hammer head can rotate. The second point is less obvious and comes from the fact that piano technicians clearly divide the hammer head's felt into several zones that are provided with different cares during the "needling" operation. It consists in penetrating needles in the hammer felt (see figure 11(b)) in order to change its mechanical properties. In piano maintenance textbooks, three zones are identified, where the needling must be different (see figure 11(c)). Consequently, the coefficients of the hammer head - string interaction could be modeled as a function of the contact point on the hammer head's surface. Unfortunately, to the best of our knowledge, this kind of experimental data is not available in the literature and would be very difficult to calibrate manually.

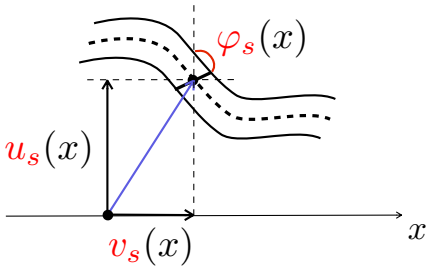

(a) Variables considered in the string model. Transversal displacement u_s (m), longitudinal displacement v_s (m), shear angle φ_s (rad).

(b) Hammer voicing with a needle voicing tool. From piesikpiano.com.

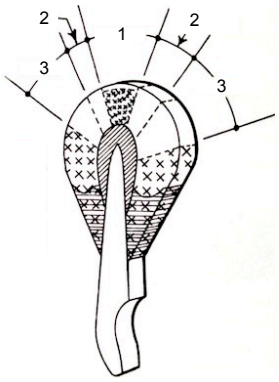

(c) Hammer head needling zones. Zone 1 : weak - light needling for piano dynamics. Zone 2 : medium - deep needling for mezzo-forte dynamics. Zone 3 : heavy - deep needling for forte dynamics. From [20].

Figure 11: String model variables and theory of hammer voicing.

5. Conclusions

In this paper, novel energy-preserving numerical schemes were provided for a Timoshenko beam in non-forced unknown rotation. Numerical simulations were carried out for the application case of a vibrating piano hammer shank coupled to a hammer head, coupled to a whole piano. To our knowledge, this work provides the first numerical simulation of such a complete system. Thanks to this simulation tool, we were able to highlight the effect of different pianistic touches, modeled with several input forces to the system (Jack forces). These numerical results show that the pianistic touch clearly influences the spectrum of the piano sound of equally loud isolated notes. These differences do not come from a possible shock excitation on the structure, nor from a changing impact point, nor a "longitudinal rubbing motion" on the string, since neither of these features are modeled in our study. Possible extensions of this work would be to refine the let-off model in order to make it smoother, and to consider the effect of hammer head's movements on the string: a possible transmission to the strings of the horizontal motion of the hammer head, a potential change of the impact point on the string, or even a change in the hammer stiffness coefficients if the contact point on the hammer's head surface were to vary.

Acknowledgments

Experiments presented in this paper were carried out using the PLAFRIM experimental testbed, being developed under the Inria PlaFRIM development action with support from LABRI and IMB and other entities: Conseil Régional d'Aquitaine, FeDER, Université de Bordeaux and CNRS (see https://plafrim.bordeaux.inria.fr/). Computer time for this study was also provided by the computing facilities MCIA (Mésocentre de Calcul Intensif Aquitain) of the Université de Bordeaux and of the Université de Pau et des Pays de l'Adour.

Appendix A. Derivation of the model : virtual work principle

In this appendix we explain all terms involved in the virtual work identity.

Appendix A.1. Acceleration

The virtual work coming from acceleration has two contributions : from the shank and from the head.
The calculus is completed from the expression of the second-derivative of $\mathbf{r}$:

$$\ddot{\mathbf{r}} = \left[-\tau\,\ddot{\varphi}\cos\varphi + \tau\,\dot{\varphi}^2\sin\varphi - (s-\tau\sin\varphi)\,\dot{\theta}^2 + 2(\dot{w}-\tau\,\dot{\varphi}\sin\varphi)\,\dot{\theta} + (w+\tau\cos\varphi)\,\ddot{\theta}\right]\mathbf{u}_r + \left[2\,\tau\,\dot{\varphi}\cos\varphi\,\dot{\theta} - (s-\tau\sin\varphi)\,\ddot{\theta} + \ddot{w} - \tau\,\ddot{\varphi}\sin\varphi - \tau\,\dot{\varphi}^2\cos\varphi - (w+\tau\cos\varphi)\,\dot{\theta}^2\right]\mathbf{u}_\theta$$

and the virtual displacement $\delta\mathbf{r}$:

$$\delta\mathbf{r} \;=\; \left[-z\,\delta\varphi\cos\varphi + (w+z\cos\varphi)\,\delta\theta\right]\mathbf{u}_r \;+\; \left[-(x-z\sin\varphi)\,\delta\theta + \;(\delta w - z\,\delta\varphi\;\sin\varphi)\right]\mathbf{u}_\theta$$

The values of φ are assumed to be very small (Timoshenko hypotheses), the following substitutions are performed :

$$\cos\varphi \;\approx\; 1, \quad \sin\varphi \;\approx\; \varphi$$

Therefore, the second-derivative of $\mathbf{r}$ is approximated as:

$$\ddot{\mathbf{r}} \;=\; \left[-\tau\,\ddot{\varphi} - s\,\dot{\theta}^2 + 2\,\dot{w}\,\dot{\theta} + (w+\tau)\,\ddot{\theta}\right]\mathbf{u}_r \;+\; \left[2\,\tau\,\dot{\varphi}\,\dot{\theta} - s\,\ddot{\theta} + \ddot{w} - \tau\,\dot{\varphi}^2 - (w+\tau)\,\dot{\theta}^2\right]\mathbf{u}_\theta$$

and the virtual displacement:

$$\delta\mathbf{r} \;=\; \left[-\tau\,\delta\varphi + (w+\tau)\,\delta\theta\right]\mathbf{u}_r + \left[-s\,\delta\theta + \delta w\right]\mathbf{u}_\theta$$

The integral of 1 on the section of the beam is equal to A the area of this section, the integral of τ equal to 0 (due to symmetry) and the integral of τ^2 is equal to I the bending moment of inertia of the beam. For instance, in the case of a circle cross-section, we have

$$A = \pi R^2 \quad \text{and} \quad I = \frac{\pi R^4}{4}, \quad \text{where } R \text{ is the radius.}$$

The virtual work due to the beam acceleration is then equal to:

$$\mathcal{P}_{\text{acc}}(\mathbf{r}) = \iiint \rho\, \ddot{\mathbf{r}} \cdot \delta\mathbf{r} \approx \int \rho A \left(-s\,\ddot{\theta} + \ddot{w} - w\,\dot{\theta}^2\right)\, \delta w + \int \rho I\,(\ddot{\varphi} - \ddot{\theta})\, \delta\varphi + \int \rho A \left(w^2\,\ddot{\theta} + 2\,w\,\dot{w}\,\dot{\theta} + s^2\,\ddot{\theta} - s\,\ddot{w}\right)\, \delta\theta + \int \rho I \left(\ddot{\theta} - \ddot{\varphi}\right)\, \delta\theta$$

and the virtual work due to the head acceleration is

$$\mathcal{P}_{\text{acc}}(\boldsymbol{\xi}) = m_H\, \ddot{\boldsymbol{\xi}} \cdot \delta\boldsymbol{\xi}$$

Appendix A.2. Exterior forces on the shank

The gravity field applies at each point of the beam:

$$\mathbf{F}_{\text{grav,shank}} = -\rho\, g\, {}^t(0, 1, 0) = -\rho\, g \sin\theta\, \mathbf{u}_r \;+\; \rho\, g \cos\theta\, \mathbf{u}_\theta$$

So the virtual work of gravity on the beam reads:

$$\mathcal{P}_{\text{grav,shank}} = \iiint \mathbf{F}_{\text{grav,shank}} \cdot \delta\mathbf{r} = \int -\rho A g \sin\theta\, [w\delta\theta] + \int \rho A g \cos\theta\, [\delta w - s\delta\theta]$$

The jack force is located at point $x = x_{\text{jack}}$ and oriented along $-\mathbf{u}_\theta$:

$$\mathbf{F}_{\text{jack}} = -F_{\text{jack}}\, \delta_{\text{jack}}(s)\, \mathbf{u}_\theta \quad \Rightarrow \quad \mathcal{P}_{\text{jack}} = \int -F_{\text{jack}}\, \delta_{\text{jack}}(s)\, (\delta w - s\delta\theta)$$

The coupling force with the head is located on the center of gravity of the head and acts on the last point of the shank. It has to be written in terms of shank's unknowns:

$$\begin{aligned}
\mathcal{P}_{\text{coupl,shank}} &= \mathbf{F}_{\text{coupl}} \cdot \delta\boldsymbol{\xi} \\
&= [(w(L) - H)\, \delta\theta]\, \mathbf{F}_{\text{coupl}} \cdot \mathbf{u}_r \;+ [-L\delta\theta + \;(\delta w(L))]\, \mathbf{F}_{\text{coupl}} \cdot \mathbf{u}_\theta \\
&= \delta\theta \left[(w(L) - H) \left(\mathbf{F}_{\text{coupl}} \cdot \mathbf{u}_r\right) - L \left(\mathbf{F}_{\text{coupl}} \cdot \mathbf{u}_\theta\right)\right] + \delta w(L) \left(\mathbf{F}_{\text{coupl}} \cdot \mathbf{u}_\theta\right)
\end{aligned}$$

Appendix A.3. Exterior forces on the head

Gravity applies to the head's mass:

$$\mathcal{P}_{\text{grav,shank}} = -m_H\, g\, \mathbf{u}_y \cdot \delta\boldsymbol{\xi}$$

Furthermore, the opposite of the coupling force acts back on the head:

$$\mathcal{P}_{\text{coupl,shank}} = -\mathbf{F}_{\text{coupl}} \cdot \delta\boldsymbol{\xi}$$

We take into account the force applied by the string:

$$\mathcal{P}_{\text{string}} = F_{\text{string}}\, \mathbf{u}_y \cdot \delta\boldsymbol{\xi}$$

F_{string} is considered as a given force amplitude.

Appendix A.4. Interior forces

The interior forces of the beam come from the elastic deformation. Under the hypothesis of a linear Hooke's law, and following the literature (see [11]), we write:

$$\mathcal{P}_{\text{int}} = \int AG\kappa\, (\partial_s w - \varphi)\, \partial_s\, (\delta w) - \int AG\kappa\, (\partial_s w - \varphi)\, \delta\varphi + \int EI \partial_s\varphi\, \partial_s\, (\delta\varphi)$$

Appendix B. Proof of consistency of system (12) with the inertial terms

We see that equation (12b) is not the natural consistent approximation of the continuous terms, but comes from the variational integration technique. Consistency is not obvious and can be shown as follows. We perform a Taylor expansion on the exact solution in order to evaluate the truncation error:

$$\begin{aligned}\frac{\theta^{n+1}-\theta^n}{\Delta t} &= \frac{1}{\Delta t}\left[\cancel{\theta(t^n)} + \Delta t\dot\theta(t^n) + \frac{\Delta t^2}{2}\ddot\theta(t^n) + \frac{\Delta t^3}{6}\dddot\theta(t^n) - \cancel{\theta(t^n)} + O(\Delta t^4)\right]\\ &= \dot\theta(t^n) + \frac{\Delta t}{2}\ddot\theta(t^n) + \frac{\Delta t^2}{6}\dddot\theta(t^n) + O(\Delta t^3)\end{aligned}$$

$$\begin{aligned}\left(\frac{w^{n+1}+w^n}{2}\right)^2 &= \left[w(t^n) + \frac{\Delta t}{2}\,\dot w(t^n) + \frac{\Delta t^2}{4}\ddot w(t^n) + O(\Delta t^3)\right]^2\\ &= w^2(t^n) + \Delta t\,\dot w(t^n)w(t^n) + \frac{\Delta t^2}{4}\left(\dot w^2(t^n) + 2w(t^n)\ddot w(t^n)\right) + O(\Delta t^3)\end{aligned}$$

$$\begin{aligned}\Rightarrow\left(\frac{\theta^{n+1}-\theta^n}{\Delta t}\right)\left(\frac{w^n+w^{n-1}}{2}\right)^2 &= w^2(t^n)\dot\theta(t^n) + \Delta t\left[\frac{1}{2}\ddot\theta(t^n)w^2(t^n) + \dot w(t^n)\,w(t^n)\,\dot\theta(t^n)\right]\\ &+ \Delta t^2\left[\frac{1}{6}\dddot\theta(t^n)w^2(t^n) + \frac{1}{2}\ddot\theta(t^n)\dot w(t^n)\,w(t^n) + \frac{1}{4}\dot\theta(t^n)\left(\dot w^2(t^n) + 2w(t^n)\ddot w(t^n)\right)\right] + O(\Delta t^3)\end{aligned}$$

In the same way, $$\frac{\theta^n-\theta^{n-1}}{\Delta t} = \dot\theta(t^n) - \frac{\Delta t}{2}\ddot\theta(t^n) + \frac{\Delta t^2}{6}\dddot\theta(t^n) + O(\Delta t^3)$$

$$\left(\frac{w^n+w^{n-1}}{2}\right)^2 = w^2(t^n) - \Delta t\,\dot w(t^n)w(t^n) + \frac{\Delta t^2}{4}\left(\dot w^2(t^n) + 2w(t^n)\ddot w(t^n)\right) + O(\Delta t^3)$$

$$\begin{aligned}\Rightarrow\left(\frac{\theta^n-\theta^{n-1}}{\Delta t}\right)\left(\frac{w^n+w^{n-1}}{2}\right)^2 &= w^2(t^n)\dot\theta(t^n) - \Delta t\left[\frac{1}{2}\ddot\theta(t^n)w^2(t^n) + \dot w(t^n)\,w(t^n)\,\dot\theta(t^n)\right]\\ &+ \Delta t^2\left[\frac{1}{6}\dddot\theta(t^n)w^2(t^n) + \frac{1}{2}\ddot\theta(t^n)\dot w(t^n)\,w(t^n) + \frac{1}{4}\dot\theta(t^n)\left(\dot w^2(t^n) + 2w(t^n)\ddot w(t^n)\right)\right] + O(\Delta t^3)\end{aligned}$$

Finally, we obtain the consistency of (12b):

$$\frac{1}{\Delta t}\left[\frac{\theta^{n+1}-\theta^n}{\Delta t}\left(\frac{w^{n+1}+w^n}{2}\right)^2 - \frac{\theta^n-\theta^{n-1}}{\Delta t}\left(\frac{w^n+w^{n-1}}{2}\right)^2\right] = w^2(t^n)\ddot\theta(t^n) + 2\dot w(t^n)\,w(t^n)\,\dot\theta(t^n) + O(\Delta t^2)$$

Consistency of the discretisation (12a) is straightforward.

References

[1] G. W. Koornhof and A. J. van der Walt, The influence of touch on piano sound, Proceedings of the Stockholm Music Acoustics Conference (SMAC'93), Stockholm, Sweden, vol. 79, pp 302–308, 1994.

[2] W. Goebl, R. Bresin, A. Galembo, Once again: The perception of piano touch and tone. Can touch audibly change piano sound independently of intensity ?, Proceedings of the International Symposium on Musical Acoustics (ISMA2004), Nara, Japan, pp 1–4, 2004.

[3] A. Askenfelt and E. V. Jansson, From touch to string vibrations. II: The motion of the key and hammer, J. Acoust. Soc. Am. vol. 90(5), pp 2383–2393, 1991.

[4] N. Giordano and J. P. Winans II, Piano hammers and their force compression characteristics: Does a power law make sense ?, J. Acoust. Soc. Am., vol. 107(4), pp 2248–2255, 2000.

[5] S. Birkett, Experimental investigation of the piano hammer-string interaction, J. Acoust. Soc. Am., vol. 133(4), pp 2467–2478, 2013.

[6] A. Izadbakhsh, J. McPhee, and S. Birkett, Dynamic Modeling and Experimental Testing of a Piano Action Mechanism With a Flexible Hammer Shank, J. Comput. Nonlinear Dynam., vol. 3(031004), pp 1–10, 2008.
[7] C. P. Vyasarayani and S. Birkett and J. McPhee, Modeling the dynamics of a compliant piano action mechanism impacting an elastic stiff string, J. Acoust. Soc. Am., vol. 125(6), pp 4034-4042, 2009.
[8] J. Chabassier, A. Chaigne and P. Joly, Modeling and simulation of a grand piano, J. Acoust. Soc. Am., vol. 134(1), pp 648–665, 2013.
[9] S. Timoshenko and S. Woinowsky-Krieger, Theory of plates and shells, Second Edition, McGraw Hill Book Company, New York, 1959.
[10] R Dautray, JL Lions, C Bardos, M Cessenat, P Lascaux, A Kavenoky, B Mercier, O Pironneau, B Scheurer, and R Sentis. Mathematical analysis and numerical methods for science and technology - vol. 6. Springer, 2000.
[11] S. C. Lin and K. M. Hsiao, Vibration analysis of a rotating Timoshenko beam, Journal of Sound and Vibration, vol. 240(2), pp 303–322, 2001.
[12] D. Chapelle, An optimal low-order locking-free finite element method for Reissner-Mindlin plates, Math. Models Methods Appl. Sci, vol. 8(3), pp 407–430, 1998.
[13] A. Quarteroni and R. Sacco and F. Saleri, Méthodes Numériques, Springer Verlag, France, 2000.
[14] A. Lew and J. E. Marsden and M. Ortiz and M. West, Variational time integrators, Int. J. Numer. Meth. Eng., vol. 60, pp 153–212, 2004.
[15] J. Chabassier and S. Imperiale, Stability and dispersion analysis of improved time discretization for simply supported prestressed Timoshenko systems. Application to the stiff piano string, Wave Motion, vol. 50(3), pp 456-480, 2013.
[16] H. Fletcher and E. Blackham, Quality of piano tones, J. Acoust. Soc. Am., vol. 34(6), pp 749–761, 1962.
[17] G. Cohen and P. Grob, Higher Order Spectral Finite Elements for Reissner-Mindlin Equations in the Time Domain, SIAM J. Sci. Comput., vol. 29(3), pp 986-1005, 2007.
[18] J. Chabassier and M. Duruflé, Physical parameters for piano modeling, Inria technical report, RT-425, pp 1–24, 2012.
[19] J. Chabassier, A. Chaigne and P. Joly, Energy preserving schemes for nonlinear Hamiltonian systems of wave equations: Application to the vibrating piano string, Computer Methods in Applied Mechanics and Engineering, vol. 199, pp 2779–2795, 2010.
[20] A. A. Reblitz, Le piano. Entretien, Accord & Restauration, L'entretemps (second french edition), France, pp 212 , 2005.

List of Figures